Published in final edited form as:
Aging Cell. 2012 October ; 11(5): 770–782. doi:10.1111/j.1474-9726.2012.00843.x.

Dietary restriction attenuates age-associated muscle atrophy by lowering oxidative stress in mice even in complete absence of CuZnSOD

Young C. Jang[1,4,8], **Yuhong Liu**[1,4], **Christopher R. Hayworth**[6], **Arunabh Bhattacharya**[1,4], **Michael S. Lustgarten**[2,4], **Florian L. Muller**[1,4], **Asish Chaudhuri**[3,4,5], **Wenbo Qi**[1,4,5], **Yan Li**[1,4,5], **Jing-Yi Huang**[7], **Eric Verdin**[7], **Arlan Richardson**[1,4,5], and **Holly Van Remmen**[1,4,5]

[1]Department of Cellular and Structural Biology, University of Texas Health Science Center at San Antonio, San Antonio, Texas 78229

[2]Department of Physiology, University of Texas Health Science Center at San Antonio, San Antonio, Texas 78229

[3]Department of Biochemistry, University of Texas Health Science Center at San Antonio, San Antonio, Texas 78229

[4]Barshop Institute for Longevity and Aging Studies, University of Texas Health Science Center at San Antonio, San Antonio, Texas 78229

[5]South Texas Veterans Health Care System, San Antonio, Texas 78229

[6]Section of Neurobiology and Institute for Neuroscience, University of Texas, Austin, Texas 78712

[7]Gladstone Institute of Virology and Immunology, University of California, San Francisco, San Francisco, California 94158

Abstract

Age-related loss of muscle mass and function, sarcopenia, has a major impact on the quality of life in the elderly. Among the proposed causes of sarcopenia are mitochondrial dysfunction and accumulated oxidative damage during aging. Dietary restriction (DR), a robust dietary intervention that extends lifespan and modulates age-related pathology in a variety of species has been shown to protect from sarcopenia in rodents. Although the mechanism(s) by which DR modulates aging are still not defined, one potential mechanism is through modulation of oxidative stress and mitochondrial dysfunction. To directly test the protective effect of DR against oxidative stress induced muscle atrophy *in vivo*, we subjected mice lacking a key antioxidant enzyme, CuZnSOD (*Sod1*) to DR (40% of *ad libitum* fed diet). We have previously shown that the *Sod1*$^{-/-}$ mice exhibit an acceleration of sarcopenia associated with high oxidative stress, mitochondrial dysfunction, and severe neuromuscular innervation defects. Despite the dramatic atrophy phenotype in the *Sod1*$^{-/-}$ mice, DR led to a reversal or attenuation of reduced muscle function, loss of innervation and muscle atrophy in these mice. DR improves mitochondrial function as evidenced by enhanced Ca^{2+} regulation and reduction of mitochondrial reactive oxygen species (ROS). Furthermore, we show upregulation of SIRT3 and MnSOD in DR animals, consistent with

Corresponding author: Holly Van Remmen, Ph.D. The Sam and Ann Barshop Institute for Longevity and Aging Studies, University of Texas Health Science Center at San Antonio, 15355 Lambda Drive San Antonio, Texas 78245-3207, Phone: (210) 562-6141, Fax: (210) 562-6110, vanremmen@uthscsa.edu.
[8]Current Address: Department of Stem Cell & Regenerative Biology and Harvard Stem Cell Institute, Harvard University, Cambridge, Massachusetts 02138

Supplemental information The supplemental information includes, five supplemental figures and supplemental materials and methods.

reduced mitochondrial oxidative stress and reduced oxidative damage in muscle tissue measured as F_2- isoprostanes. Collectively, our results demonstrate that DR is a powerful mediator of mitochondrial function, mitochondrial ROS production, and oxidative damage, providing a solid protection against oxidative stress induced neuromuscular defects and muscle atrophy *in vivo* even under conditions of high oxidative stress.

INTRODUCTION

Age-related loss of muscle mass and function, referred to as sarcopenia, is a significant problem that has serious implications for quality of life in the elderly. The etiology of sarcopenia is multifaceted and involves a number of intrinsic and extrinsic factors (1). In recent years, accumulating evidence has pointed to mitochondrial dysfunction as one of the key driving force in the progression of sarcopenia (2–4). More specifically, mitochondrial production of reactive oxygen species (ROS) and the concomitant increase in oxidative damage to protein, lipids, and nucleic acids have been implicated as one of the mechanisms of muscle atrophy during aging (3, 4). However, the exact mechanism by which increased ROS and elevated oxidative damage leads to a decrease in muscle mass and muscle fiber deterioration during aging are not fully understood.

One critical aspect of the initiation and progression of muscle atrophy during aging is changes in innervation of muscle during aging. Innervation by the motor neurons is essential for maintenance of skeletal muscle size, fiber type, structure, and function. It has been well documented that degeneration of motor neurons, followed by changes in structural and functional integrity of the neuromuscular junction (NMJ) and loss of motor units contribute significantly to the progression of skeletal muscle aging (5, 6). Recently, we and others have shown that oxidative stress and mitochondrial dysfunction may be directly linked to increased denervation seen in senescent animals (2, 7, 8). Specifically, we have demonstrated that in different models of denervation, the mitochondrial ROS generation is strongly correlated with the extent of muscle atrophy (8). Moreover, mitochondrial dysfunction at the postsynaptic site may have additional debilitating effect on denervation by oxidative modification of key proteins in the NMJ assembly as well as altering bioenergetic\function and calcium regulation that are vital for synaptic transmission.

Dietary restriction (DR) or calorie restriction (CR) without malnutrition is the only non-genetic intervention that consistently extends lifespan in diverse species and delays the onset of numerous age-related phenotypes including sarcopenia (1, 4, 9–12). The anti-aging effect of DR at the biochemical level has been attributed to a reduction of oxidative damage and preservation of mitochondrial structural and functional integrity (10, 13, 14). For example, CR has been reported to reduce mitochondrial proton leak and superoxide generation from the mitochondrial complex I and complex III of electron transport chain (ETC) (15–17). CR also has been shown to increase antioxidant genes that are responsible for scavenging ROS (18). Moreover, CR can alter fatty acid composition, making it more resistant to lipid peroxidation of mitochondrial membrane during aging in skeletal muscle (19). Interestingly, a recent report demonstrated that CR can attenuate age-associated structural changes in the NMJ (20). These observations suggest a link between mitochondrial dysfunction, oxidative damage, and denervation in aging skeletal muscle. However, most of the data supporting these views are correlation and a direct link between mitochondrial dysfunction, oxidative stress, and neuromuscular innervation has not been established. Thus, to investigate the direct beneficial role of DR against mitochondrial dysfunction, oxidative stress, and denervation *in vivo*, we fed mice that lack the key antioxidant enzyme, CuZnSOD (*Sod1*), a restricted diet (60% of the amount consumed by *ad libitum* fed mice). *Sod1*$^{-/-}$ mice have previously been shown to have elevated levels of oxidative stress, mitochondrial dysfunction, severe neuromuscular innervation defects and an acceleration of age-related

atrophy. Here, we provide direct evidence that DR is a powerful dietary intervention that can protect against oxidative damage-induced muscle atrophy, even under conditions of elevated oxidative stress.

RESULTS

Dietary restriction (DR) attenuates age-related muscle atrophy

The protective effects of caloric or dietary restriction on age-related muscle atrophy have been shown in a number of studies using rats and a small number of studies using mice (21–23). In the current study, we measured the effect of long-term DR on age-related muscle loss in the C57BL6 strain of mice. We compared the wet-weight of muscle isolated from young adult (11 months), old (33 months), and old (33 months) mice that were fed a 40% DR diet. In agreement with previous reports (4, 21, 22), both the gastrocnemius and quadriceps muscles showed a significant ($p<0.001$) improvement against age-associated muscle atrophy in mice fed a DR diet (Figure 1A and Figure 1B). Old *ad libitum* fed mice showed over a 30% loss in gastrocnemius muscle mass, while age matched DR mice showed less than 15% atrophy. Next, we examined changes in the ultrastructure of myofibers during aging using transmission electron microscopy (TEM). When compared to the gastrocnemius muscle from young mice, muscles from old mice show a marked increase in myofibrillar degeneration (Figure 1C). In addition, myofibrils in gastrocnemius from old mice show an increase in abnormal intrafibrillar mitochondria. In contrast, in age-matched old mice on the DR diet there is a remarkable reduction in myofibrillar degeneration and fewer abnormal mitochondria (Figure 1C). Intriguingly, in muscle from old mice, many postsynaptic mitochondria surrounding the neuromuscular junction (NMJ) have an abnormal swollen appearance; whereas in old DR muscle, large abnormal postsynaptic mitochondria were absent and their morphology was similar to that of young muscle (Figure 1D). These data suggest that the DR diet provides a robust protection against age-associated mitochondrial defects. Furthermore, TEM also revealed that the morphology of neuromuscular junction (NMJ) undergoes a dramatic alteration during aging that includes; shrinkage of the synaptic cleft and reduced size of the postsynaptic terminals. Strikingly, DR reversed these changes and maintained the structure of the NMJ with advanced aging (Figure 1D). To further investigate the age-associated changes in the NMJs, we performed immunofluorescence staining of NMJ to assess morphological changes during aging in light microscope level. In confirmation of our EM results; the NMJ in gastrocnemius muscle from old mice displayed a marked decrease in the size of the presynaptic endplate and the postsynaptic terminal as well as structural changes such as fragmentation and sprouting compared to NMJ from gastrocnemius of young mice. In stark contrast, NMJ from age-matched DR mice maintained structural integrity and size, in agreement with the EM results (Figure 1E–F). The endplate size was reduced by nearly 50% in old *ad libitum* fed mice, but the endplates were maintained at normal size in the old mice on DR. Given that mitochondria are the major source of ROS generation, we next assessed the oxidative stress status in skeletal muscle tissue by measuring muscle F_2-isoprostane as a maker of lipid peroxidation. Indeed, F_2-isoprostane levels were nearly doubled in gastrocnemius muscle from old mice compared to young mice, yet old age-matched DR mice displayed a significantly reduced level of oxidative damage. Thus, we postulated that DR maintains muscle mass during aging by lowering oxidative damage and preserving mitochondrial function, elements that are critical for neuromuscular interaction. However, these observations are correlation and a cause-effect relationship cannot be established. Therefore, in order to directly test the causative relation of DR on oxidative damage and muscle mass, we analyzed the same parameters using CuZnSOD (*Sod1*) knockout mice. We have previously shown that mice lacking *Sod1* have very high levels of oxidative stress and an acceleration of sarcopenia due to mitochondrial dysfunction, and denervation (2, 8, 24).

Dietary restriction (DR) attenuates oxidative stress induced muscle atrophy in Sod1 null mice

We measured body weight changes of WT, *Sod1*$^{-/-}$, and *Sod1*$^{-/-}$ mice on the restricted diet (*Sod1*$^{-/-}$DR) mice as a function of lifespan. We observed that throughout the lifespan, *Sod1*$^{-/-}$ DR mice maintain a smaller body weight (approximately 25% lower) compared to age-matched *Sod1*$^{-/-}$ and WT mice. In addition, as reported in previous studies, *Sod1*$^{-/-}$ mice are smaller than WT littermates (2, 24). However, body weight remains consistent throughout the lifespan in *Sod1*$^{-/-}$ DR mice and by 600–800 days of age there is no difference in body mass between *Sod1*$^{-/-}$ and *Sod1*$^{-/-}$ DR mice (Figure 2A). Next, in order to determine whether DR attenuated loss of muscle mass with age in *Sod1*$^{-/-}$ mice, we compared the wet-weight of hindlimb muscles in *Sod1*$^{-/-}$ and *Sod1*$^{-/-}$ DR mice. Because the mice on DR are smaller in bodyweight, gastrocnemius muscle was normalized to body mass. *Sod1*$^{-/-}$ muscle from mice on DR showed a significant protection against muscle atrophy throughout their lifespan (Figure 2B). Furthermore, as animals reached the age of 400–600 days, even the absolute wet-weight of DR mice was larger compared to age-matched *ad libitum* fed *Sod1*$^{-/-}$ mice, demonstrating a significant attenuation of age-dependent loss of muscle mass (Figure S1). In parallel to the wet-weight results, the cross-sectional area of gastrocnemius muscle measured at 14 months of age showed a significant decrease in *Sod1*$^{-/-}$ mice, while the cross-sectional area in gastrocnemius muscle from *Sod1*$^{-/-}$ DR mice was similar to the area in WT mice (Figure S2, Figure2C, and 2F). In addition, muscle from *Sod1*$^{-/-}$ mice showed an increased prevalence of fibrotic fibers as measured by Gomori trichrome staining. On the other hand, in muscle from *Sod1*$^{-/-}$ DR mice, only a minimal amount of fibrosis was detected at 14 months (Figure 2D and Figure 2G). Muscles from *Sod1*$^{-/-}$ mice also show a dramatic increase in centralized nuclei suggesting degeneration and regeneration of fibers are occurring in these fibers. Similarly, muscle from the *Sod1*$^{-/-}$ DR mice, the number of regenerating fibers was significantly diminished (Figure 2E and 2H). Interestingly, when muscle fibers were stained with cytochrome c oxidase (COX) to identify oxidative fibers, fibers from *Sod1*$^{-/-}$ mice, but not *Sod1*$^{-/-}$ DR mice, have a high number of COX positive fibers that are clustered together (Figure 2E). This phenomenon is known as ‘fiber-type grouping’ which is commonly seen during normal aging process. It has been documented that fiber-type grouping results from remodeling of motor neurons when muscle fibers are denervated and reinnervated by sprouting of neighboring motor axon (5, 6). These results prompted us to test whether DR is also protective against the severe denervation observed in *Sod1*$^{-/-}$ muscle.

Dietary restriction (DR) attenuates neuromuscular degeneration in Sod1 null mice

Consistent with the results of our previous study, *Sod1*$^{-/-}$ mice show a marked increase in denervated muscle fibers with age (2). To investigate whether DR can ameliorate muscle atrophy by reducing denervation, we analyzed the morphology of NMJ in gastrocnemius muscle in mice of different ages by immunofluorescence staining. As depicted in Figure 3A and 3C, muscle from *Sod1*$^{-/-}$ mice shows severe alterations in motoneurons and presynaptic terminals at 14 months compared to muscle from WT mice. Axons show alterations associated with denervation such as thinning, sprouting, and swollen varicosities at the presynaptic terminal. It should be noted that the presence of these thin axons could also be interpreted as evidence of recently grown axons seeking reinnervation. In addition, as revealed by EM, in *Sod1*$^{-/-}$, prevalence of decreased myelinated and small motoneurons significantly increased with age (Figure 3B). On the postsynaptic side, AChRs show a marked elevation in the number of fragmented and small endplates (Figure 3C). Consistent with our previous report (2), the percentage of innervated NMJ is reduced nearly 70% in the *Sod1*$^{-/-}$ mice (Figure S4B). In contrast, muscles from *Sod1*$^{-/-}$ DR mice show less features of denervation, a restoration of endplate size, less fragmented NMJs and a higher number of innervated NMJs (Figure 3A, 3C and 3D). To evaluate the impact of these changes in NMJ

morphology on overall neurological function of WT, *Sod1*$^{-/-}$, and *Sod1*$^{-/-}$ DR mice at 11 months of age, we used an accelerating rotarod test. In agreement with the NMJ alterations, the *Sod1*$^{-/-}$ mice showed a significant deficit in rotarod performance compared to WT mice. Surprisingly, the DR diet enhanced the performance of the WT mice as well as the *Sod1*$^{-/-}$ mice (Figure 3E). In support of these results, EM images of NMJs revealed changes in NMJs in *Sod1*$^{-/-}$ mice that are similar to those seen in normal aging, including a reduced synaptic cleft and smaller endplate size, which DR was able to reverse to a significant degree. Furthermore, we found an increase in the number of mitochondria surrounding NMJs in gastrocnemius muscle from *Sod1*$^{-/-}$ mice at 14 months of age, as well as an increased prevalence of swollen mitochondria with vacuoles, indicative of mitochondrial dysfunction. DR reduced the number of abnormal postsynaptic mitochondria in gastrocnemius of the *Sod1*$^{-/-}$ DR mice (Figure 3F). Post-synaptic mitochondria not only generate ATP required for synaptic transmission and excitation-contraction coupling, but also play a pivotal role in buffering excessive cytosolic Ca^{2+} during these processes (6). Therefore, we postulated that increased oxidative stress during aging and in *Sod1* deficient mice may lead to alterations in mitochondrial Ca^{2+} homeostasis, which can further exacerbate mitochondrial dysfunction and hence mitochondrial ROS generation causing a feed forward mechanism of muscle and NMJ deterioration.

Dietary restriction (DR) attenuates mitochondrial dysfunction in Sod1 null mice

Mitochondrial Ca^{2+} uptake is dependent on the ability of mitochondria to maintain membrane potential. To test whether alterations in mitochondrial Ca^{2+} homeostasis contributes to muscle and NMJ deterioration in the *Sod1*$^{-/-}$ mice, we measured the cytosolic Ca^{2+} and mitochondrial membrane potential ($\Delta\Psi m$) in live single fibers isolated from flexor digitorum brevis (FDB) muscle of WT, *Sod1*$^{-/-}$, and *Sod1*$^{-/-}$ DR mice at 11–12 months of age using confocal microscopy. As expected, in muscle from *Sod1*$^{-/-}$ mice, there was a significant increase in cytosolic Ca^{2+} compared to WT, whereas age-matched *Sod1*$^{-/-}$ DR mice display a remarkable reduction in cytosolic Ca^{2+} to the level of WT mice. Similarly, the mitochondrial membrane potential was markedly declined in *Sod1*$^{-/-}$ muscle compared to WT and *Sod1*$^{-/-}$ DR muscle fibers (Figure 4A). To confirm these results, we assessed the mitochondrial Ca^{2+} uptake capacity in freshly purified mitochondria from gastrocnemius muscle at 11–12 months. As illustrated in Figure 4B, in mitochondria isolated from *Sod1*$^{-/-}$ muscle, time to permeability transition pore (PTP) opening, where mitochondria Ca^{2+} uptake reaches its threshold, was significantly shorter than in mitochondria from WT gastrocnemius muscle. Consistently, DR was able to completely reverse the decline in Ca^{2+} uptake of *Sod1*$^{-/-}$ mitochondria (Figure 4B and 4C). Furthermore, there are a large number of swollen interfibrillar mitochondria with altered cristae structure in gastrocnemius muscle from *Sod1*$^{-/-}$ mice, while in muscle from *Sod1*$^{-/-}$ DR mice these were completely absent (Figure 4D). These results support a role of Ca^{2+} dysregulation in mitochondrial function in the *Sod1*$^{-/-}$ mice.

It has been well documented that uncontrolled level of Ca^{2+} leads to increased generation of ROS by the mitochondrial electron transport chain (ETC). Therefore, we analyzed mitochondrial ROS generation by H_2O_2 emission using isolated mitochondria from hindlimb muscle at different age points. As shown in Figure 5A, in state 1, where no mitochondrial substrates were added, *Sod1*$^{-/-}$ showed a 3-fold higher increase in H_2O_2 emission compared to WT. Remarkably, DR was able to completely reduce H_2O_2 generation to the WT level in both young (7–12 months) and old (18–22 months) age. When complex I-linked substrate, glutamate/malate (Figure 5B) and complex II-linked substrate (succinate/rotenone)(data not shown) were added to increase the electron flow, only the aged (18–22 months) showed similar results as State I respiration. Likewise, when the free radical leak was estimated by normalizing ROS emission to the amount oxygen consumed, leak was

elevated in muscle mitochondria from *Sod1* null mice and DR reversed this trend (Figure 5C). To further assess the overall oxidative damage, we measured F_2-isoprostane levels at 14 months of age. Consistent with the mitochondrial ROS data, the F_2-isoprostane was elevated in $Sod1^{-/-}$ compared to WT, but DR completely reversed the damage to WT level. In an effort to more fully understand the robust protective effect of DR against oxidative stress in the mitochondria, we next asked whether the antioxidant enzymes were upregulated by DR. (Figure 5E). However, none of the antioxidant enzyme we tested showed any significant difference except, mitochondrial MnSOD.

Dietary restriction (DR) upregulates MnSOD in Sod1 null mice

MnSOD, which is the main mitochondrial antioxidant enzyme responsible for scavenging superoxide generated by the mitochondrial ETC, was significantly lowered in both activity and content in $Sod1^{-/-}$ muscle, whereas in $Sod1^{-/-}$ DR activity and contents were slightly restored (Figure 6A). In addition, aconitase, an enzyme that is highly reactive to superoxide due to its FeS cluster, was significantly decreased in content by loss of *Sod1*. There was a slight trend for an increase in aconitase level by DR, but it failed to reach statistical significance. Moreover, lon protease, a mitochondrial protease that cleaves oxidized aconitase for degradation, did not show any differences in *Sod1* deficiency or by DR (Figure 6A). This suggests that the increase in oxidative stress targets specific proteins and not all mitochondrial proteins are affected. Recent evidence also suggests that DR dramatically alters mitochondrial function by changing the status of lysine acetylation of key mitochondrial proteins. This is achieved by upregulation of mitochondrial sirtuin, SIRT3 (25). SIRT3 has been shown to play an important role in controlling ATP level by interacting with the subunit of complex I in mitochondrial ETC (26). Moreover, recent studies demonstrated that MnSOD is activated by SIRT3 via deactylation (27, 28). Therefore, to investigate whether protective effect of DR is related to alterations in the level of acetylated protein in $Sod1^{-/-}$ muscle, we assessed the total protein acetylation in purified muscle mitochondria from 14 month-old mice. $Sod1^{-/-}$ showed a significant increase in overall acetylated proteins compared to WT. On the other hand, in mitochondria from $Sod1^{-/-}$ DR mice, there was a significant reduction in total acetylated proteins compared to *ad libitum* fed $Sod1^{-/-}$, suggesting increased deacetylation activity with DR (Figure 6D and 6E). In parallel to these results, the SIRT3 content in $Sod1^{-/-}$ was drastically reduced whereas in $Sod1^{-/-}$ DR SIRT3 was increased to the WT level. These observations indicate that the protective effect of DR in $Sod1^{-/-}$ is possibly modulated at least in part through the upregulation of SIRT3 in the muscle mitochondria (Figure 6D and 6F). Recent evidence suggests that similar to cytosolic SIRT1, SIRT3 can also induce mitochondrial biogenesis by activating peroxisome proliferator-activated receptor gamma coactivator-1α (PGC-1α) and AMP-activated protein kinase (AMPK) in skeletal muscle. Indeed we found a significant increase in PGC-1α level in the DR $Sod1^{-/-}$ skeletal muscle (Figure 6G). Finally, to test the effect of oxidative stress on overall oxidative capacity of animals, we assessed the run-to-exhaustion test on a motorized treadmill at 11–14 months. As expected, $Sod1^{-/-}$ mice revealed a severe deficit in endurance capacity compared to WT type. On the contrary, age-matched $Sod1^{-/-}$ DR mice were able to run a significantly longer distance compared to $Sod1^{-/-}$ mice and in fact $Sod1^{-/-}$ DR mice ran close to the distance measured in the age-matched WT mice.

DISCUSSION

In summary, we demonstrate that DR is a powerful intervention that can protect against oxidative damage-induced muscle atrophy, even in a complete absence of an important antioxidant enzyme CuZnSOD. It has been well documented that DR exerts its anti-aging effect by improving mitochondrial function and by reducing mitochondrial ROS generation

and thus oxidative damage. However, most of the data that support this notion are correlative and the direct evidence on how DR modulates oxidative stress have been lacking. In this study, we report for the first time that DR directly attenuates age-related loss of muscle mass by improving mitochondria function, which in turn, lowers the mitochondrial ROS production. The loss of *Sod1* exacerbates age-related decline in muscle function and severe muscle atrophy displayed in *Sod1*$^{-/-}$ mice were associated with increased fibrosis as well as an increase in the number of regenerating myofibers, suggesting endogenous damage and repair are activated in *Sod1*$^{-/-}$ muscle. These changes were also seen in normal aging muscle. A large amount of literature has suggested that the regenerative potential of skeletal muscle declines with age and that this impairment is associated with an increase in tissue fibrosis (29, 30). The fact that these changes were completely reversed by DR suggests that DR may be also improving regenerative potential of skeletal muscle. It will be interesting to test whether muscle stem cell are impaired by oxidative stress during aging and whether DR can improve stem cell function by lowering oxidative stress during regeneration.

Innervation of skeletal muscle fibers by motor neuron is critical for maintenance of muscle size, structure, and function. It has been well documented that the loss of motor units and denervation advances with normal aging in muscle (5, 6). Age-dependent loss of muscle mass seen in *Sod1*$^{-/-}$ mice is most likely due to loss of innervation and loss of motor neurons. A previous study demonstrated that expression of the SOD1 gene targeted to motor neuron in *Sod1 null* background prevented the axonal neuropathy seen these animals, demonstrating the critical importance of oxidative stress regulation and protection against oxidative damage in motor neurons (31). Indeed, *Sod1*$^{-/-}$ mice have a significant reduction in motor axon number as measured by Nissl staining, whereas *Sod1*$^{-/-}$ DR showed no difference compared to WT (Figure S2). Moreover, based on EM, DR was able to attenuate morphological alterations of motor neuron, such as thinning of myelinated sheets and vacuole formation (Figure S2). Several studies also have noted that alterations in NMJ are responsible for increased denervation seen old animals and humans (6, 32, 33). A recent report by Valdez *et al* also characterized changes in aging NMJ and demonstrated that long-term calorie restriction significantly decreased the incidence of structural alterations including axonal swelling, sprouting, synaptic detachment, and fragmentation of postsynaptic sites, further validating our results in this study (20).

A key result of our study is evidence for a potential mechanistic basis for the ability of DR to maintain neuromuscular innervation by enhancing mitochondrial function. First, DR maintains mitochondrial function by limiting mitochondrial ROS production. In our previous study we identified that mitochondrial H_2O_2 production correlates strongly with innervation and degree of muscle atrophy in different models of denervation (34). Additionally, in the peripheral synapse, H_2O_2 has been shown to inhibit the quantal release of acetylcholine and vesicle fusion (35). Furthermore, key proteins that constitute NMJ synapse as well as subsynaptic nuclei, that are localized around NMJ and specialized specifically for gene expression for NMJ, might be oxidatively modified and damaged by excess ROS and lose their function during aging and in *Sod1*$^{-/-}$ muscle. Second, the maintenance of mitochondrial function by DR may offer protection against disruption in Ca^{2+} homeostasis during aging and in *Sod1*$^{-/-}$ mice. It has been well documented that mitochondria play a pivotal role as a Ca^{2+} sink. Cytosolic Ca^{2+} levels are tightly regulated in skeletal muscle for contractile activity, gene expression, and many other functions (36). It has been reported that calpain, a Ca^{2+} dependent protease, plays an important role in the clustering of AChR by interacting with rapsyn. We have previously reported that calpain levels are significantly elevated in *Sod1*$^{-/-}$ muscle, indirectly supporting the elevation cytosolic Ca^{2+} (2). Collectively, these observations, coupled with the fact that mitochondria are clustered around the postsynaptic site, imply that increased mitochondrial dysfunction during aging may be the critical factors that contribute to the progression of age-related

deterioration of NMJ and muscle atrophy. In support of this view, Dupuis *et al* reported that ectopically overexpressing uncoupling protein (UCP1) in muscle to chronically depolarize mitochondrial membrane potential, was enough to dismantle NMJ and triggers distal motor neuron degeneration (37). More intriguingly, in $SOD1^{G93A}$ mutant mouse model of amyotrophic lateral sclerosis (ALS), mitochondria surrounding the NMJs are selectively depolarized in ALS and these depolarized mitochondria show greater susceptibility of osmotic stress-induced Ca^{2+} activity. These authors concluded that the loss of mitochondrial regulated Ca^{2+} signaling may contribute to the progression of muscle atrophy in ALS (38).

Another potential molecular mechanism by which DR modulates mitochondrial function and mitochondrial oxidant production is through upregulation of Sirt3. A recent study demonstrated that Sirt3 can reversibly binds to the subunit of mitochondrial ETC complex I to regulate ATP levels and exposure to complex I inhibitor, rotenone or H_2O_2 *in vitro* led to a dissociation of Sirt3 from complex I. Given that *Sod1*$^{-/-}$ muscle mitochondria generate high superoxide anion from complex I, it is possible that oxidative modification of Complex I may hinder the binding of Sirt3 and alter its function. Moreover, the protective effect against oxidative stress is diminished in mice that lack Sirt3 and has been demonstrated to directly modulate MnSOD function by deacetylating its active sites (27, 28). Furthermore, DR has been also shown to upregulate phosphorylation of AMPK in skeletal muscle and conversely, in Sirt3 knockout AMPK, CREB, and PGC-1α were downregulated, suggesting that Sirt3 may also signal downstream cellular factors that modulate mitochondrial biogenesis (39). Consistent with this, several studies have demonstrated a beneficial effect of DR in skeletal muscle that includes activation of SIRT3, PGC-1α/AMPK, and MnSOD (20, 27, 39). Indeed, we also observed a significant elevation in PGC-1α mRNA level with CR in *Sod1*$^{-/-}$ muscle but not in *ad libitum* fed *Sod1*$^{-/-}$ muscle (Figure S5). Given that Sirt3 protein levels are significantly decreased in *Sod1*$^{-/-}$muscle, it is possible that downstream signaling that activates mitochondrial biogenesis may be disrupted in *Sod1*$^{-/-}$ muscle. Future studies will determine whether overexpression of Sirt3 alone has similar beneficial effect on sarcopenia and explore the therapeutic strategies to activates Sirt3.

In conclusion, we have shown that DR is a powerful modulator of age-related sarcopenia through its actions on maintenance of mitochondrial function and control of oxidative damage, even in conditions of high oxidative stress. The protective effects of DR on mitochondria contribute to the preservation of neuromuscular junction morphology, innervation of muscle fibers, and maintenance of muscle mass and structure.

MATERIALS AND METHODS

Animals

C57BL/6J mice aging colonies were maintained under specific pathogen-free conditions, housed 3–4/cage, maintained in a 12:12 (light: dark) cycle at 22 ± 2°C and 50 ± 10% relative humidity. The *Sod1*$^{-/-}$ mice have been previously described (3, 40). In our colony, the median lifespan of *Sod1*$^{-/-}$ mice is ~23 months. Unless indicated otherwise 11–14 month old female mice were used in all of the experiments. For collecting skeletal muscle, mice were euthanized using a CO_2 chamber followed by cervical dislocation. All procedures were approved by the Institutional Animal Care and Use Committee at the University of Texas Health Science Center at San Antonio and the Audie L. Murphy Veterans Hospital.

Dietary restriction

In this study, we used dietary restriction (DR) regimen where food intake was reduced by 40% as opposed to calorie restriction (CR) which uses fortified diet where calorie is reduced

by 40% but other contents (i.e. minerals, vitamin) are constant. Details of DR feedings were previously described (41).

Histology

Gastrocnemius muscle was embedded in paraffin and sectioned (10 μm) from the midbelly then stained with hematoxylin and then with eosin (H&E). For fibrosis staining, trichrome staining kit (Dako) was used following manufacturer's protocol. Images were visualized and captured with Nikon Element software (Nikon Inc.).

Electron microscopy

Muscle blocks (1 mm^3 in size) with 2% paraformaldehyde and 2.5% gluteraldehyde in 0.1 M sodium cacodylate buffer, post-fixed with 1% osmium tetroxide followed by 1% uranyl acetate. The blocks were then dehydrated through a graded series of ethanol washes and embedded in resin. Blocks were cut in ultrathin (80 nm) sections on Reichert Ultracut UCT, stained with uranyl acetate followed by lead citrate and viewed on a JEOL 1230 EX transmission electron microscope at 80kV.

Neuromuscular junction imaging

NMJ immufluorescence have been previously described (2). Briefly, thin sectioned Gastrocnemius or tibialis anterior (TA) muscles were fixed and whole mounted onto slides. To label axons, AChRs, and muscle fibers, rabbit polyclonal antibodies againstneurofilament (1:500; Chemicon) and synaptophysin (1:5; Zymed), Alexa 488-conjugated goat anti-rabbit IgG, Alexa 594-conjugated α-bungaratoxin (1:500; Invitrogen), and Alexa647-conjugated phalloidin(1:100; Invitrogen) were used. Imageswere captured at room temperature using Nikon Eclipse TE2000-U microscope (Nikon, Inc.) with 20X NA 0.5 PlanFluor or 40X 0.75 PlanFluor objective and images were analyzed with Nikon Element software (NIS element BR3.2).

Immunoblot analysis

Protein extracts were separated using standard Western blot protocol. Blots were visualized and scanned on a Typhoon 9400 (Amersham: Piscataway, NJ). Quantification of the immunoblots was performed with ImageQuant Software (Sunnyvale, CA).

Isolation of the skeletal muscle mitochondria

Mitochondria were purified from hindlimb muscle as previously described (3).

Mitochondrial H_2O_2 release

Mitochondrial ROS production was measured with the Amplex Red method (Molecular Probes, Eugene, OR) as described previously (42).

ATP production

ATP production by mitochondria was measured as previously described (3).

Single Fiber Analyses

Intact flexor digitorum brevis (FDB) muscles were surgically removed and placed in a Tyrode buffer (140 mM NaCl, 5 mM KCl, 10 mM HEPES, 2mM $MgCl_2$, 0.2 mM EGTA, pH 7.2) solution containing 0.2% type IV collagenase (Sigma C-5138, St Louis, MO) for 45 min at 37 °C. After two washes in Tyrode buffer, muscle fibers were gently dissociated by several passages through a series of Pasteur pipettes of gradually decreasing diameter. Individual FDB muscle fibers were plated onto ΔTC3 glass-bottomed Petri dishes (Fisher

Scientific, Pittsburgh, PA) in an isotonic balanced salt solution and used for imaging within 6 h. Cytosolic Ca^{2+} was measured using Fluo-4 (Invitrogen) and mitochondrial membrane potential ($\Delta\Psi m$) was measured using tetramethylrhodamine methyl ester (TMRM) (Invitrogen) using Olympus Fluoview 2000 confocal microscope with 20X Plan water immersion NA 1.0 objective at room temperature.

Mitochondrial Ca^{2+} retention capacity

To determine the maximum amount of Ca^{2+} required for mPTP opening, freshly isolated mitochondria were monitored using the membrane-impermeable fluorescent probe calcium green-5N (Invitrogen).

Statistics

The results are expressed as means ± SEM. One-way ANOVA with Tukey's *post-hoc* test were used when comparing differences. Differences were considered significant at $p<0.05$.

Supplementary Material

Refer to Web version on PubMed Central for supplementary material.

Acknowledgments

We would like to thank Dr. Ting Ting Huang for providing *Sod1 null* breeders, Dr. Noah Weisleder and Dr. Pie Lin for their help with *in vivo* electroporation, and Marian Sabia, Amanda Jernigan, Barbara Hunter, Vivian Diaz, Jimmy Wewer, and Dr. Victoria Frohlich for their technical support. Some of the images were generated in the Core Optical Imaging Facility and EM Facility which are supported by UTHSCSA, NIH-NCI P30 CA54174 (CTRC at UTHSCSA) and NIH-NIA P01AG19316. Also supported by P01AG020591 (HVR, AR, SVB, LL) and a Julie Martin Mid-Career grant from the American Federation for Aging Research (HVR).

References

1. Marzetti E, Lees HA, Wohlgemuth SE, Leeuwenburgh C. Sarcopenia of aging: underlying cellular mechanisms and protection by calorie restriction. Biofactors. 2009; 35:28–35. [PubMed: 19319843]
2. Jang YC, Lustgarten MS, Liu Y, Muller FL, Bhattacharya A, Liang H, Salmon AB, Brooks SV, Larkin L, Hayworth CR, et al. Increased superoxide in vivo accelerates age-associated muscle atrophy through mitochondrial dysfunction and neuromuscular junction degeneration. FASEB J. 2010; 24:1376–1390. [PubMed: 20040516]
3. Mansouri A, Muller FL, Liu Y, Ng R, Faulkner J, Hamilton M, Richardson A, Huang TT, Epstein CJ, Van Remmen H. Alterations in mitochondrial function, hydrogen peroxide release and oxidative damage in mouse hind-limb skeletal muscle during aging. Mech Ageing Dev. 2006; 127:298–306. [PubMed: 16405961]
4. Weindruch R. Interventions based on the possibility that oxidative stress contributes to sarcopenia. J Gerontol A Biol Sci Med Sci. 1995; 50(Spec No):157–161. [PubMed: 7493211]
5. Faulkner JA, Larkin LM, Claflin DR, Brooks SV. Age-related changes in the structure and function of skeletal muscles. Clin Exp Pharmacol Physiol. 2007; 34:1091–1096. [PubMed: 17880359]
6. Jang YC, Van Remmen H. Age-associated alterations of the neuromuscular junction. Exp Gerontol. 2011; 46:193–198. [PubMed: 20854887]
7. Kostrominova TY, Pasyk KA, Van Remmen H, Richardson AG, Faulkner JA. Adaptive changes in structure of skeletal muscles from adult Sod1 homozygous knockout mice. Cell Tissue Res. 2007; 327:595–605. [PubMed: 17109119]
8. Muller FL, Song W, Jang YC, Liu Y, Sabia M, Richardson A, Van Remmen H. Denervation-induced skeletal muscle atrophy is associated with increased mitochondrial ROS production. Am J Physiol Regul Integr Comp Physiol. 2007; 293:R1159–1168. [PubMed: 17584954]

9. Anderson RM, Barger JL, Edwards MG, Braun KH, O'Connor CE, Prolla TA, Weindruch R. Dynamic regulation of PGC-1alpha localization and turnover implicates mitochondrial adaptation in calorie restriction and the stress response. Aging Cell. 2008; 7:101–111. [PubMed: 18031569]
10. Anderson RM, Weindruch R. Metabolic reprogramming, caloric restriction and aging. Trends Endocrinol Metab. 2010; 21:134–141. [PubMed: 20004110]
11. Civitarese AE, Carling S, Heilbronn LK, Hulver MH, Ukropcova B, Deutsch WA, Smith SR, Ravussin E. Calorie restriction increases muscle mitochondrial biogenesis in healthy humans. PLoS Med. 2007; 4:e76. [PubMed: 17341128]
12. Colman RJ, Anderson RM, Johnson SC, Kastman EK, Kosmatka KJ, Beasley TM, Allison DB, Cruzen C, Simmons HA, Kemnitz JW, et al. Caloric restriction delays disease onset and mortality in rhesus monkeys. Science. 2009; 325:201–204. [PubMed: 19590001]
13. Drew B, Phaneuf S, Dirks A, Selman C, Gredilla R, Lezza A, Barja G, Leeuwenburgh C. Effects of aging and caloric restriction on mitochondrial energy production in gastrocnemius muscle and heart. Am J Physiol Regul Integr Comp Physiol. 2003; 284:R474–480. [PubMed: 12388443]
14. Mayhew M, Renganathan M, Delbono O. Effectiveness of caloric restriction in preventing age-related changes in rat skeletal muscle. Biochem Biophys Res Commun. 1998; 251:95–99. [PubMed: 9790913]
15. Bevilacqua L, Ramsey JJ, Hagopian K, Weindruch R, Harper ME. Long-term caloric restriction increases UCP3 content but decreases proton leak and reactive oxygen species production in rat skeletal muscle mitochondria. Am J Physiol Endocrinol Metab. 2005; 289:E429–438. [PubMed: 15886224]
16. Bua EA, McKiernan SH, Wanagat J, McKenzie D, Aiken JM. Mitochondrial abnormalities are more frequent in muscles undergoing sarcopenia. J Appl Physiol. 2002; 92:2617–2624. [PubMed: 12015381]
17. Hagopian K, Harper ME, Ram JJ, Humble SJ, Weindruch R, Ramsey JJ. Long-term calorie restriction reduces proton leak and hydrogen peroxide production in liver mitochondria. Am J Physiol Endocrinol Metab. 2005; 288:E674–684. [PubMed: 15562252]
18. Sreekumar R, Unnikrishnan J, Fu A, Nygren J, Short KR, Schimke J, Barazzoni R, Nair KS. Effects of caloric restriction on mitochondrial function and gene transcripts in rat muscle. Am J Physiol Endocrinol Metab. 2002; 283:E38–43. [PubMed: 12067840]
19. Cefalu WT, Wang ZQ, Bell-Farrow AD, Terry JG, Sonntag W, Waite M, Parks J. Chronic caloric restriction alters muscle membrane fatty acid content. Exp Gerontol. 2000; 35:331–341. [PubMed: 10832054]
20. Valdez G, Tapia JC, Kang H, Clemenson GD Jr, Gage FH, Lichtman JW, Sanes JR. Attenuation of age-related changes in mouse neuromuscular synapses by caloric restriction and exercise. Proc Natl Acad Sci U S A. 2010; 107:14863–14868. [PubMed: 20679195]
21. Payne AM, Dodd SL, Leeuwenburgh C. Life-long calorie restriction in Fischer 344 rats attenuates age-related loss in skeletal muscle-specific force and reduces extracellular space. J Appl Physiol. 2003; 95:2554–2562. [PubMed: 12972444]
22. McKiernan SH, Bua E, McGorray J, Aiken J. Early-onset calorie restriction conserves fiber number in aging rat skeletal muscle. FASEB J. 2004; 18:580–581. [PubMed: 14734642]
23. Renganathan M, Delbono O. Caloric restriction prevents age-related decline in skeletal muscle dihydropyridine receptor and ryanodine receptor expression. FEBS Lett. 1998; 434:346–350. [PubMed: 9742952]
24. Muller FL, Song W, Liu Y, Chaudhuri A, Pieke-Dahl S, Strong R, Huang TT, Epstein CJ, Roberts LJ 2nd, Csete M, et al. Absence of CuZn superoxide dismutase leads to elevated oxidative stress and acceleration of age-dependent skeletal muscle atrophy. Free Radic Biol Med. 2006; 40:1993–2004. [PubMed: 16716900]
25. Schwer B, Eckersdorff M, Li Y, Silva JC, Fermin D, Kurtev MV, Giallourakis C, Comb MJ, Alt FW, Lombard DB. Calorie restriction alters mitochondrial protein acetylation. Aging Cell. 2009; 8:604–606. [PubMed: 19594485]
26. Ahn BH, Kim HS, Song S, Lee IH, Liu J, Vassilopoulos A, Deng CX, Finkel T. A role for the mitochondrial deacetylase Sirt3 in regulating energy homeostasis. Proc Natl Acad Sci U S A. 2008; 105:14447–14452. [PubMed: 18794531]

27. Qiu X, Brown K, Hirschey MD, Verdin E, Chen D. Calorie restriction reduces oxidative stress by SIRT3-mediated SOD2 activation. Cell Metab. 2010; 12:662–667. [PubMed: 21109198]
28. Ozden O, Park SH, Kim HS, Jiang H, Coleman MC, Spitz DR, Gius D. Acetylation of MnSOD directs enzymatic activity responding to cellular nutrient status or oxidative stress. Aging (Albany NY). 2011; 3:102–107. [PubMed: 21386137]
29. Conboy IM, Conboy MJ, Wagers AJ, Girma ER, Weissman IL, Rando TA. Rejuvenation of aged progenitor cells by exposure to a young systemic environment. Nature. 2005; 433:760–764. [PubMed: 15716955]
30. Brack AS, Conboy MJ, Roy S, Lee M, Kuo CJ, Keller C, Rando TA. Increased Wnt signaling during aging alters muscle stem cell fate and increases fibrosis. Science. 2007; 317:807–810. [PubMed: 17690295]
31. Flood DG, Reaume AG, Gruner JA, Hoffman EK, Hirsch JD, Lin YG, Dorfman KS, Scott RW. Hindlimb motor neurons require Cu/Zn superoxide dismutase for maintenance of neuromuscular junctions. Am J Pathol. 1999; 155:663–672. [PubMed: 10433959]
32. Balice-Gordon RJ. Age-related changes in neuromuscular innervation. Muscle Nerve Suppl. 1997; 5:S83–87. [PubMed: 9331392]
33. Oda K. Age changes of motor innervation and acetylcholine receptor distribution on human skeletal muscle fibres. J Neurol Sci. 1984; 66:327–338. [PubMed: 6530617]
34. Muller FL, Song W, Jang Y, Liu Y, Sabia M, Richardson A, Van Remmen H. Denervation-Induced Skeletal Muscle Atrophy is Associated with Increased Mitochondrial ROS Production. Am J Physiol Regul Integr Comp Physiol. 2007
35. Giniatullin AR, Darios F, Shakirzyanova A, Davletov B, Giniatullin R. SNAP25 is a pre-synaptic target for the depressant action of reactive oxygen species on transmitter release. J Neurochem. 2006; 98:1789–1797. [PubMed: 16945102]
36. Brookes PS, Yoon Y, Robotham JL, Anders MW, Sheu SS. Calcium, ATP, and ROS: a mitochondrial love-hate triangle. Am J Physiol Cell Physiol. 2004; 287:C817–833. [PubMed: 15355853]
37. Dupuis L, Gonzalez de Aguilar JL, Echaniz-Laguna A, Eschbach J, Rene F, Oudart H, Halter B, Huze C, Schaeffer L, Bouillaud F, et al. Muscle mitochondrial uncoupling dismantles neuromuscular junction and triggers distal degeneration of motor neurons. PLoS One. 2009; 4:e5390. [PubMed: 19404401]
38. Zhou J, Yi J, Fu R, Liu E, Siddique T, Rios E, Deng HX. Hyperactive intracellular calcium signaling associated with localized mitochondrial defects in skeletal muscle of an animal model of amyotrophic lateral sclerosis. J Biol Chem. 2010; 285:705–712. [PubMed: 19889637]
39. Palacios OM, Carmona JJ, Michan S, Chen KY, Manabe Y, Ward JL 3rd, Goodyear LJ, Tong Q. Diet and exercise signals regulate SIRT3 and activate AMPK and PGC-1alpha in skeletal muscle. Aging (Albany NY). 2009; 1:771–783. [PubMed: 20157566]
40. Elchuri S, Oberley TD, Qi W, Eisenstein RS, Jackson Roberts L, Van Remmen H, Epstein CJ, Huang TT. CuZnSOD deficiency leads to persistent and widespread oxidative damage and hepatocarcinogenesis later in life. Oncogene. 2005; 24:367–380. [PubMed: 15531919]
41. Ikeno Y, Hubbard GB, Lee S, Richardson A, Strong R, Diaz V, Nelson JF. Housing density does not influence the longevity effect of calorie restriction. J Gerontol A Biol Sci Med Sci. 2005; 60:1510–1517. [PubMed: 16424282]
42. Muller FL, Liu Y, Van Remmen H. Complex III releases superoxide to both sides of the inner mitochondrial membrane. J Biol Chem. 2004; 279:49064–49073. [PubMed: 15317809]

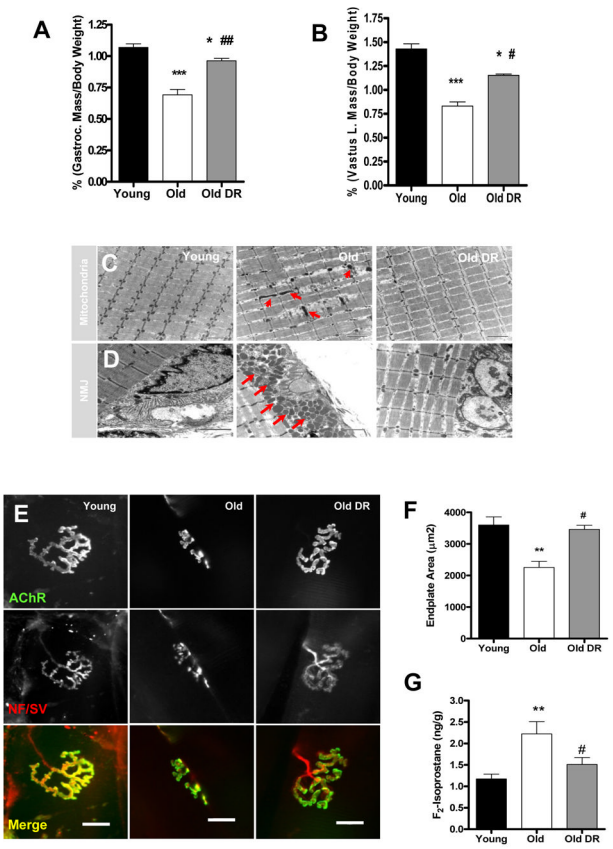

Figure 1. Calorie restriction (CR) attenuates age-related muscle atrophy

(A) A comparison of gastrocnemius (*left*) and vastus lateralis (*right*) muscle wet-weight normalized to body weight (n=6–7). (B) Transmission electron micrographs (TEM) of interfibrillar mitochondria (C) and neuromuscular junctions (D) from gastrocnemius muscle of young, old, and old DR. Arrows denote abnormal mitochondria (n=3). Scale bar=2μm (E) A representative image of neuromuscular junction from gastrocnemius muscle. Scale bar=20μm. (F) A quantification of postsynaptic endplate area. Young mice are 7 months and old mice are 33 months old (n=6). (G) Oxidative stress is reduced by DR as measured by F_2-isoprostanes as a marker of lipid peroxidation (n=6). Young *vs.* Old ***p<0.01* and Old *vs.* Old *DR* $^{\#}p<0.05$. All values are represented as mean ± SEM.

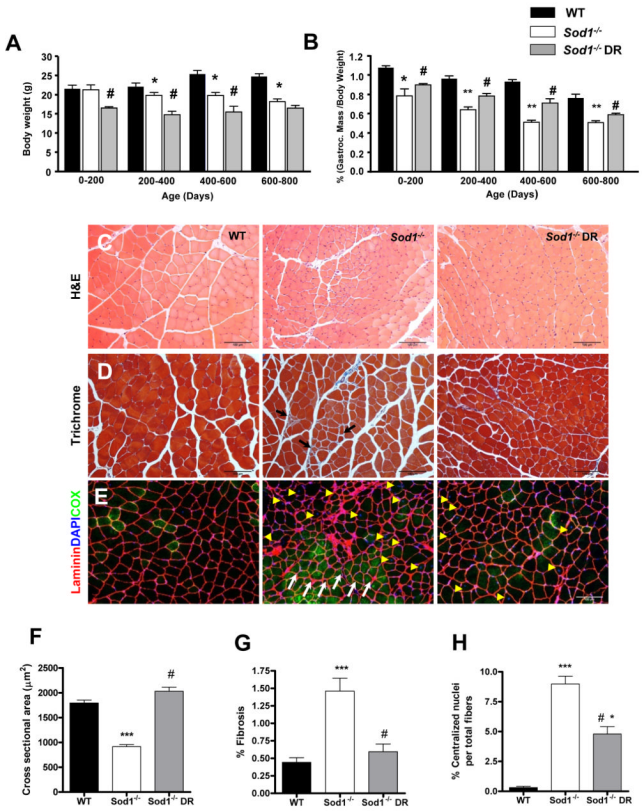

Figure 2. Dietary restriction (DR) attenuates age-related muscle atrophy and degeneration in *Sod1*$^{-/-}$ mice

(A) Bodyweight measured throughout the lifespan (n=6–8). (B) A comparison of gastrocnemius wet weight measured throughout the lifespan (n=6–8). (C–G) A comparison of morphological features of WT, *Sod1*$^{-/-}$, and *Sod1*$^{-/-}$ CR at 11–14 months. (C) A representative images of hematoxylin and eosin staining of gastrocnemius muscle (n=4). (D) A representative staining of Gomori trichrome staining of gastrocnemius muscle (n=4). Black arrows denote increased fibrosis. % Fibrosis is defined as the area of blue relative to red fiber area in a given field of view. 20–30 random fields of view were chosen for quantification. (E) A representative immunofluorescence staining of gastrocnemius muscle. Sarcolemma membrane is stained with anti-laminin pseudo colored in red, myonuclei are colored in blue using DAPI, and oxidative fibers are stained with anti-cytochrome c oxidase in green. White arrows represent fiber grouping and yellow arrowhead denote centralized nuclei (n=4). (F) A quantification of cross sectional area shown in (C). (G) A quantification of fibrotic area shown in (D). (H) A quantification of centralized nuclei shown in (E). WT *vs. Sod1*$^{-/-}$ ***$p<0.001$, *Sod1*$^{-/-}$ *vs. Sod1*$^{-/-}$ DR $^{\#}p<0.05$, and WT *vs. Sod1*$^{-/-}$ DR $^{*}p<0.05$. All values are represented as mean ± SEM.

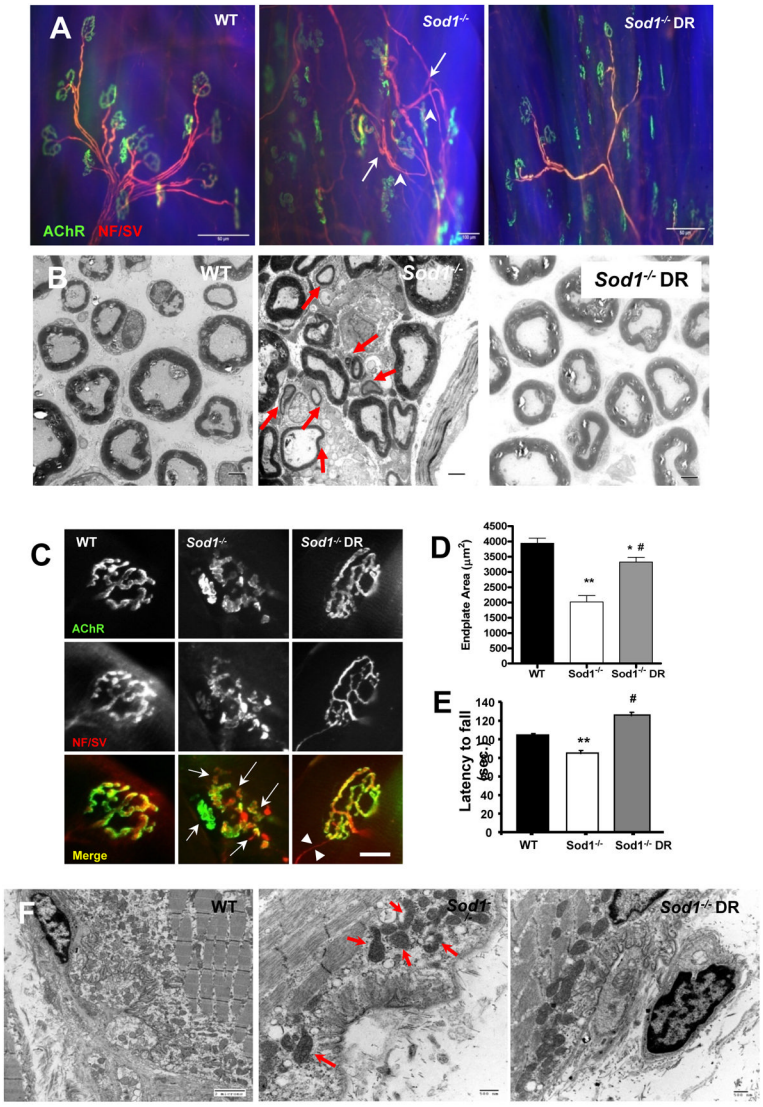

Figure 3. Dietary restriction (DR) attenuates age-related defects in neuromuscular junction (NMJ) in *Sod1*$^{-/-}$ mice

(A) A representative images of neuromuscular junction from gastrocnemius from WT, *Sod1*$^{-/-}$, and *Sod1*$^{-/-}$ DR at 11–14 months. Motoneuron and presynaptic nerve terminals were stained using anti-neurofilament and anti-synaptophysin (pseudo-colored in red) and postsynaptic acetylcholine receptors (AChR) were stained using fluorophore conjugated α-Bungarotoxin (pseudo-colored in green). Arrows denote sprouting of motoneuron and arrowheads denote thinning of motor neurons. (B) TEM of sciatic nerve cross section. Red arrows denote small demyelinated motor neurons. Scale bar=2μm (n=4) (C) Representative images of individual neuromuscular junctions. Arrows denote fragmentations of pre- and post-synaptic endplates. Scale bar = 20μm (D) A quantification of endplate area. At least 60 endplates and 10 random images per animal were scored blindly (n=4). Endplate size was measured by calculating the surface area that are colocalized by AChR (Bungarotoxin) and presynaptic motoneuron (neurofilament/synaptophysin) using Nikon Element software. (E) A comparison of rotarod performance at 16–18 months as measurement of overall neurological function (n=6). WT *vs. Sod1*$^{-/-}$ $^{**}p<0.01$, *Sod1*$^{-/-}$ *vs. Sod1*$^{-/-}$ DR $^{\#}p<0.05$, and WT *vs. Sod1*$^{-/-}$ DR $^{*}p<0.05$. (F) A representative electron micrograph images of

gastrocnemius neuromuscular junctions at 11 months. Arrows denote abnormal subsynaptic mitochondria (n=3). All values are represented as mean ± SEM.

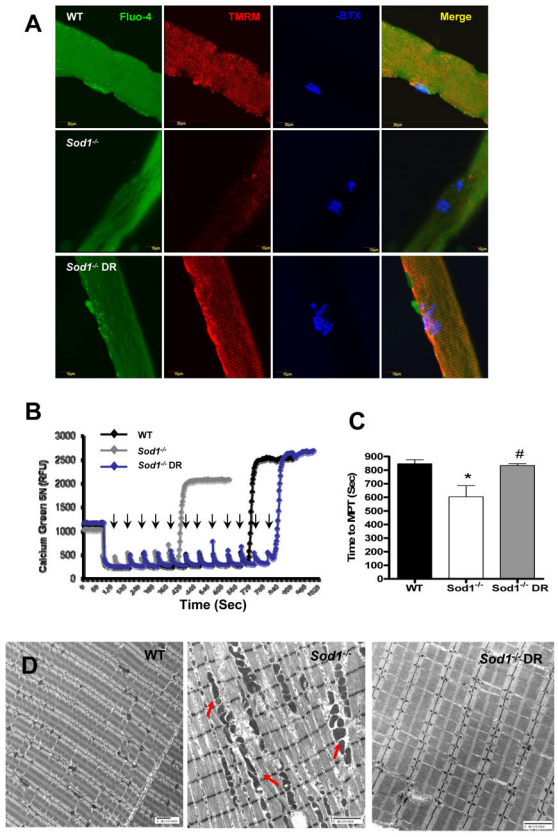

Figure 4. Dietary restriction (DR) ameliorates age-related defects in mitochondrial Ca^{2+} homeostasis in *Sod1*$^{-/-}$ mice

(A) Live cell imaging from single fibers from flexor digitorum brevis (FDB) (WT in *top panels*, *Sod1*$^{-/-}$ *middle panels*, and *Sod1*$^{-/-}$ CR *bottom panels*). Cytosolic Ca^{2+} were stained with Fluo-4 (green), mitochondrial membrane potential were assessed with tetramethylrhodamine methyl esters (TMRM) stained in red, and NMJ stained in blue with α-Bungarotoxin. Merged images of three stains shown in *right column*. At least 20 fibers were analyzed from each animal (n=5). (B) A representative traces of calcium retention assay in mitochondria isolated from hindlimb muscle at 14 months (n=5). Arrows denote number of times Ca^{2+} (2μM) was added to mitochondria. (C) A quantification of time to reach mitochondrial permeability transition (MPT) (n=6). (D) A representative electron micrograph of alterations in interfibrillar mitochondria from gastrocnemius muscle at 13–14 months (n=3). WT *vs. Sod1*$^{-/-}$ *$p<0.05$, **$p<0.01$, ***$p<0.001$, and *Sod1*$^{-/-}$ *vs. Sod1*$^{-/-}$ DR $^{\#}p<0.05$.

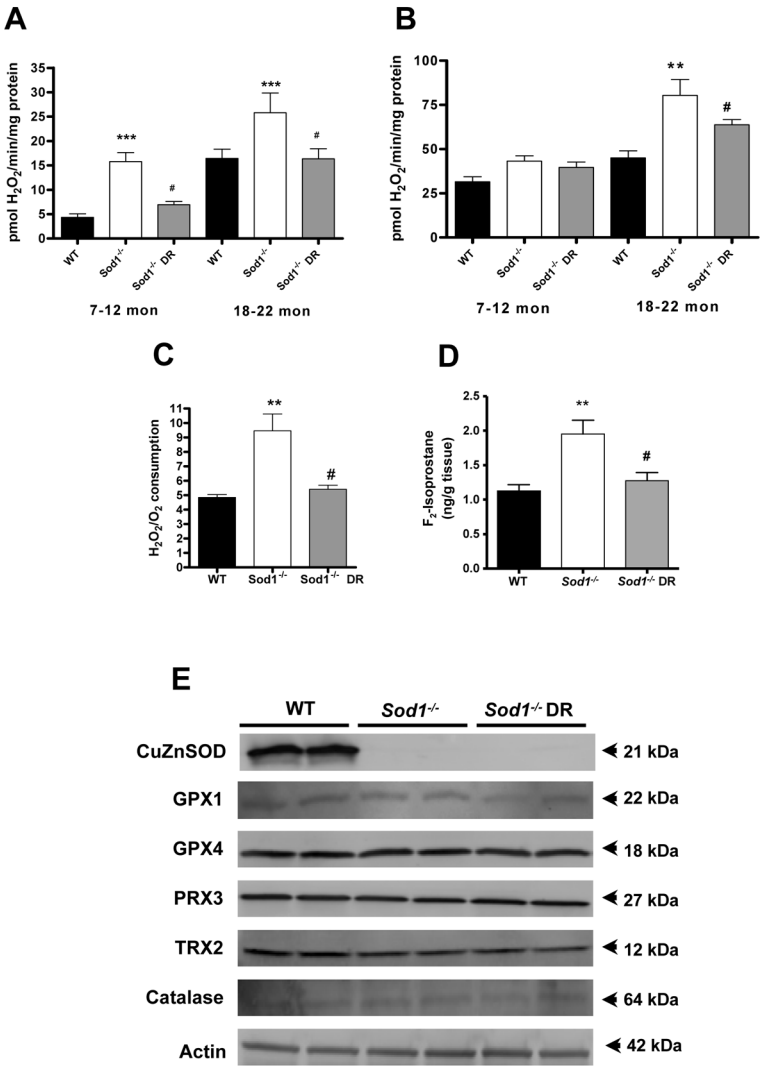

Figure 5. Dietary restriction (DR) attenuates age-related defects in mitochondrial ROS in *Sod1*$^{-/-}$ mice

(A) State 1 and (B) State 2 complex I-linked (glutamate/malate) mitochondrial H_2O_2 production at different age points (n=4–6). (C) Mitochondrial free radical leak (H_2O_2 emission/State 2 O_2 consumption) assessed from hind-limb muscle at 18 months (n=6). (D) Oxidative stress is measured by F_2-isoprostanes as a marker of lipid peroxidation (n=6). (E) Western blot analyses of different antioxidant enzymes. WT *vs. Sod1*$^{-/-}$ *$p<0.05$, **$p<0.01$, ***$p<0.001$, and *Sod1*$^{-/-}$ *vs. Sod1*$^{-/-}$ DR $^{\#}p<0.05$.

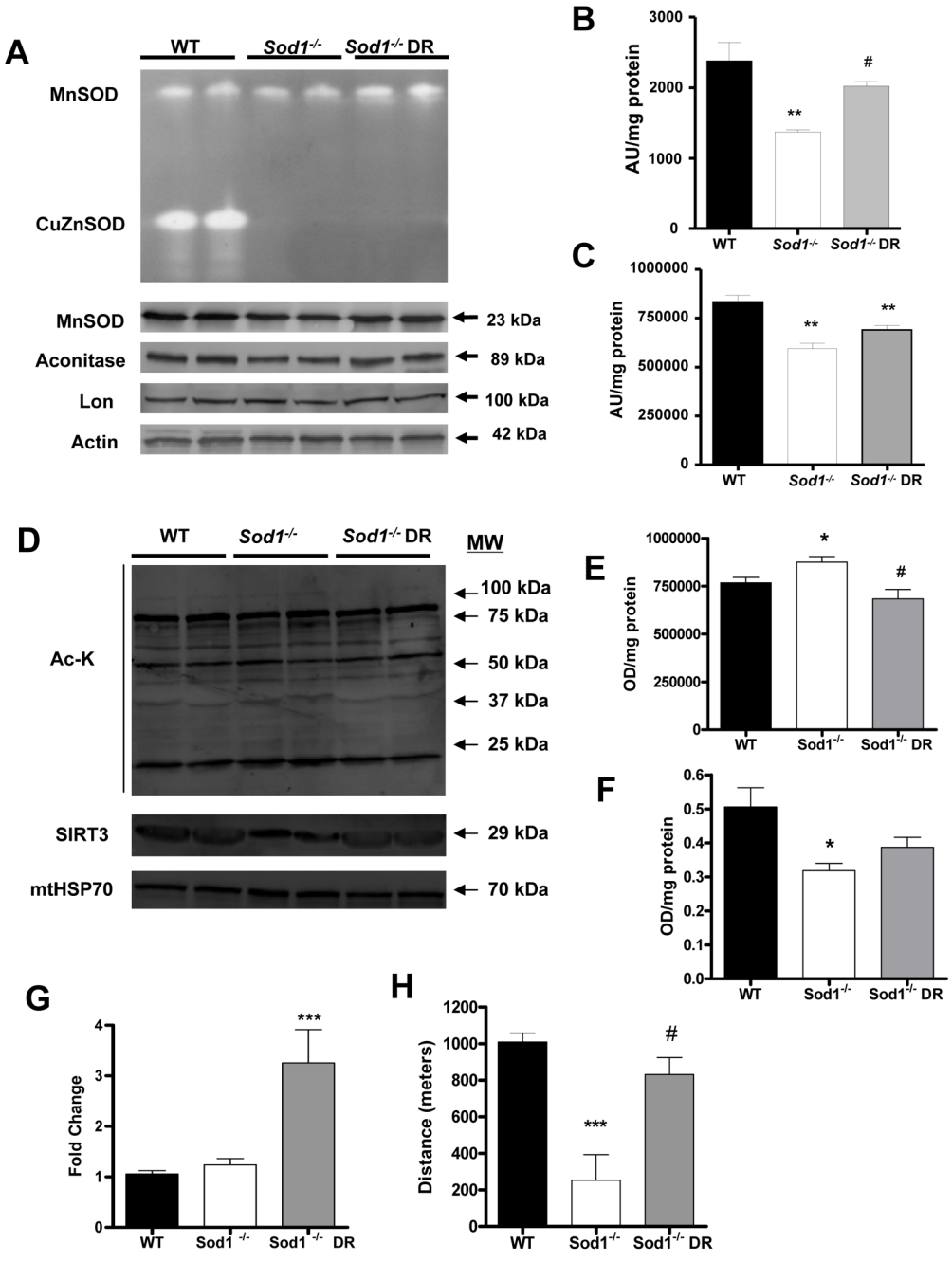

Figure 6. Dietary restriction (DR) upregulates MnSOD activity and decreases mitochondrial protein acetylation

(A) *Top*, A representative image of gel-based superoxide dismutase activity. Top band represents MnSOD (tetramer) activity and lower band represents CuZnSOD (dimer) activity. *Bottom*, Western blot analysis of MnSOD, aconitase, and lon protease (n=6). Actin was used as loading control. (B) A quantification of MnSOD activity shown in (A). (C) A quantification of aconitase content shown in (A). (D) *Top*, A representative immunoblot of total acetylated lysine residues in mitochondrial fractions. *Bottom,* A representative immunoblot of SIRT3 content (n=4). mtHSP70 was used as loading control. (E) A quantification of total acetylated lysine shown in (D) (n=5). (F) A quantification of SIRT3

content shown in (D) (n=5). (G) A quantitative real-time PCR analysis of PGC-1α. (H) Endurance exercise capacity measured at 14–16 months (n=4–5). WT *vs.* $Sod1^{-/-}$ *$p<0.05$, **$p<0.01$, $Sod1^{-/-}$ *vs.* $Sod1^{-/-}$ DR $^{\#}p<0.05$, and WT *vs.* $Sod1^{-/-}$ DR **$p<0.01$.